NANOSYSTEMS:
PHYSICS, CHEMISTRY, MATHEMATICS

Original article

Shamsuddin Ahmad, et al. *Nanosystems: Phys. Chem. Math.*, 2025, **16** (6), 763–769.
http://nanojournal.ifmo.ru
DOI 10.17586/2220-8054-2025-16-6-763-769

Defective aluminum nitride monolayer as electrode material for supercapacitor applications: a DFT study

Shamsuddin Ahmad[1], Md. Mahfoozul Haque[2], Zaheer Abbas[3], Md. Shahzad Khan[1]

[1]Department of Physics, Z. A. Islamia P. G. College Siwan, Bihar-841226, India
[2]Department of Physics, Marwari College, T. M. Bhagalpur University, Bihar-812007, India
[3]Department of Science and Humanities, Government Engineering College, Jehanabad, Bihar-804407, India

Corresponding author: Md. Shahzad Khan, kshahzad001@gmail.com

ABSTRACT This paper analyzes the quantum capacitance properties of aluminum nitride nanosheets (AlNNS) with defects focusing on their potential use in supercapacitors. We validated the structural stability of the primitive cell through cohesive energy calculations and phonon spectrum analysis. Our findings indicate that monolayers containing aluminum (Al), nitrogen (N), or with Al–N deficiencies exhibit p-type/n-type or wide bandgap semiconducting state. Calculations of defect formation energy indicate that N-deficient AlNNS is the least favorable option. The presence of under-coordinated atoms near the defect leads to the emergence of new impurity state in the forbidden energy bad gap region. This prompted us for a detailed examination of their quantum capacitance, which is heavily influenced by the density of states around the Fermi energy. Our study reveals that Al-deficient AlNNS achieves a maximum quantum capacitance ($C_{Q\text{Max}}$) of 690 μF/cm^2 in the positively biased region, making it a suitable candidate for anodic material in supercapacitor applications. In comparison, the nitrogen-deficient AlNNS reaches a $C_{Q\text{Max}}$ of 313 μF/cm^2 and a maximum surface charge capacity (Q_{Max}) of -91 μC/cm^2, highlighting its potential as a cathodic material. The Al-N-deficient AlNNS shows intermediate behavior with prominent quantum capacitance peaks in both biased regions, offering additional flexibility for potential applications.

KEYWORDS density functional theory, band structure, aluminium nitride nanosheet, quantum capacitance, surface charge

ACKNOWLEDGEMENTS No external funding or specific support was received for this research.

FOR CITATION Shamsuddin Ahmad, Md. Mahfoozul Haque, Zaheer Abbas, Md. Shahzad Khan Defective aluminum nitride monolayer as electrode material for supercapacitor applications: a DFT study. *Nanosystems: Phys. Chem. Math.*, 2025, **16** (6), 763–769.

1. Introduction

The increasing demand for electronic devices and electric vehicles has created a need for efficient electrical energy sources [1]. As environmental degradation continues, there is a heightened emphasis on eco-friendly energy solutions, such as supercapacitors. Supercapacitors are beneficial not only because they are environmentally friendly, but also due to their high energy and power densities, as well as their excellent charging and discharging capabilities [2, 3]. Researches [4–6] show that the total capacitance C of a supercapacitor electrode is determined by the series combination of two capacitances: the electric double-layer capacitance (C_{EDL}) and the quantum capacitance C_Q, as represented in equation (1):

$$\frac{1}{C} = \frac{1}{C_Q} + \frac{1}{C_{\text{EDL}}}. \tag{1}$$

From equation (1), it is evident that materials possessing a low quantum capacitance will correspondingly show a reduced total capacitance. Hence, the examining the quantum capacitance characteristics of supercapacitor electrode materials is essential. On the other hand, among materials, the aluminum nitride (AlN) possesses a large band gap, making it suitable for optoelectronic and modern electronic applications [7, 8]. At the nanoscale, AlN nanostructures are relatively obscure in terms of experimental findings. However, a few works validate the existence of nanowires, nanotubes, and nanosheets, although they remain in an early stage [9–15]. Among these nanostructures, the 2D nanosheet with a honeycomb lattice structure has attracted significant research interest [16–19]. In this study, we rigorously explore the impact of defects on the quantum capacitance of AlN nanosheets (AlNNS). Before delving into quantum capacitance (C_Q) and the derived surface charge (Q), we systematically investigate the structural stability and electronic properties of the defected monolayer. The impurity states arising from the defects are expected to introduce new energy states within the wide band gap of the AlN monolayer. These states are likely to play a vital role in describing C_Q of the nanosheet.

2. Methodology

A 5×5 hexagonal supercell consisting of 25 aluminum (Al) and 25 nitrogen (N) atoms is considered as a pristine AlNNS (Fig. 1(a)). To avoid mirror image interactions, a large lattice vector of 20 Å is selected along the Z-axis. Mono-vacancy or divacancy are created by removing either single Al/N atom or by removing the nearest Al–N bond from the thinned planar layer (Fig. 1(b,c,d)).

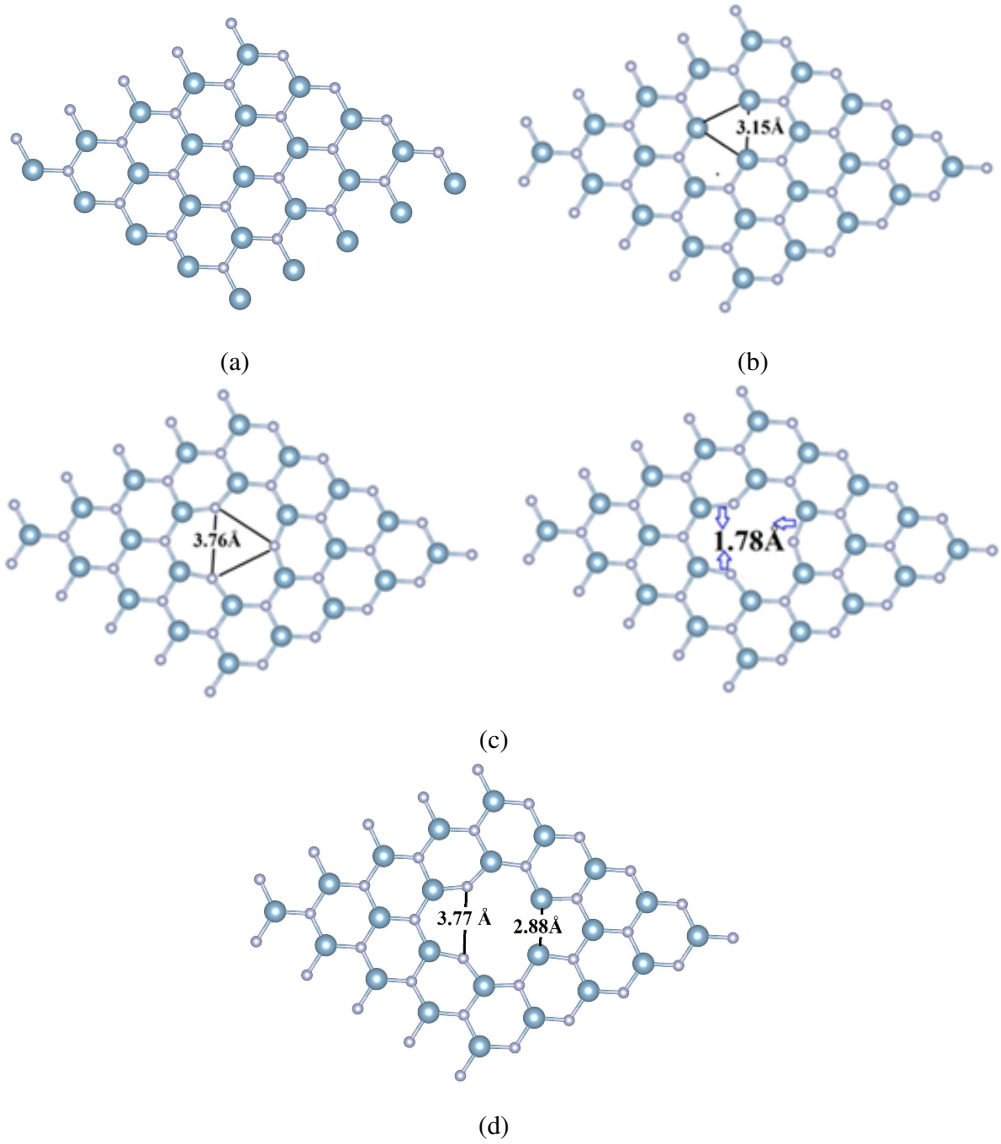

FIG. 1. a) Pristine, b) Al-deficient, c) N-deficient and d) Al–N-deficient aluminum nitride nanosheet (AlNNS)

The exchange-correlation functional used for structural optimization of both pristine and defective AlNNS are based on the Perdew, Burke, and Ernzerhof (PBE) [20] method in the frame of generalized gradient approximation (GGA). The structures are integrated over the Brillouin zone using a $7 \times 7 \times 1$ k-point Monkhorst–Pack [21] mesh, and a kinetic energy cutoff of 450 eV is employed to ensure geometric accuracy. Valence electrons are modeled with a double-zeta polarization (DZP) basis set, and conjugate gradient techniques are applied to achieve geometric perfection with residual forces below 0.05 eV/Å. For core-valence interactions, the Troullier–Martins [22] norm-conserving pseudopotential is utilized. To calculate electronic properties such as the band structure, density of states (DOS) spectra, Mulliken population analysis, and electron difference density, a high-resolution Monkhorst-Pack grid of $17 \times 17 \times 1$ is adopted. All calculations are performed using Spanish Initiative for Electronic Simulations with Thousands of Atoms (SIESTA) quantum chemical code [23, 24].

2.1. Quantum capacitance calculations

In MATLAB [25], the following mathematical expressions are used to compute the quantum capacitance (C_Q) of AlNNS:

$$C_Q = e^2 \int_{-\infty}^{\infty} D(E) F_T \left(E - e\Phi_G\right) dE. \tag{2}$$

The density of states and thermal broadening are represented by $D(E)$ and $F_T(E)$, respectively. E is the eigen-energy, while e denotes the applied bias voltage and electronic charge value. $F_T(E)$ is expressed using a specific relation:

$$F_T(E) = (4k_BT)^{-1} Sech^2(E/2k_BT), \tag{3}$$

where k_B denotes Boltzmann's constant and the standard room temperature is set at $T = 300$ K, it is important to note that an excess charge emerges when the chemical potential (μ_F) is shifted by $e\Phi_G$. This parameter can be accurately calculated using the provided expression:

$$Q = \int_{-\infty}^{\infty} D(E)[f(E) - f\left(E - e\Phi_G\right)]dE. \tag{4}$$

Here $f(E)$ denotes the Fermi–Dirac distribution function, with E representing the relative energy in relation to the Fermi level, E_F.

3. Results and discussion

3.1. Structural and electronic analysis

We initiated our investigation with a primitive hexagonal cell of aluminum nitride (AlN) with a lattice constant of 3.16 Å, a parameter selected based on previous research findings (Fig. S1) [26]. A systematic energy versus lattice constant analysis was conducted to determine the optimal configuration (Fig. S2). This analysis revealed an energy minimum at a lattice constant of 3.10 Å, which was subsequently used for further relaxation procedures. The primitive cell, consisting of one aluminum (Al) and one nitrogen (N) atom, was relaxed to achieve its ground state configuration, resulting in an Al–N bond length of 1.82 Å. The stability of this configuration was confirmed through phonon band dispersion calculations, which showed no imaginary frequencies (Fig. 2(a)). In comparison, the cohesive energy of bulk AlN in the wurtzite phase is -6.01 eV, while that of AlN nanosheet in our calculations is -5.08 eV. This suggests that the freestanding monolayer has low stability compared to bulk wurtzite-AlN. This primitive configuration has an indirect electronic bandgap of 2.92 eV, with the valence band maxima (VBM) and conduction band minima (CBM) located at the K and Γ points, respectively (Fig. 2(b)). A 5×5 AlNNS supercell is generated from the primitive cell and is subsequently relaxed using the DFT framework discussed in the methodology section. Fig. S3 illustrates the electronic band structure of the supercell, which exhibits an indirect bandgap of 2.93 eV. When an aluminium (Al) vacancy was introduced into the AlNNS, significant structural modifications were observed in the vicinity of the defect site. The ground state configuration exhibited local distortion that slightly affected the planarity of the monolayer (Fig. 1(b)). The Al–N bonds associated with under-coordinated N-atoms contracted by 0.40 Å, resulting in a reduced bond length of 1.78 Å.

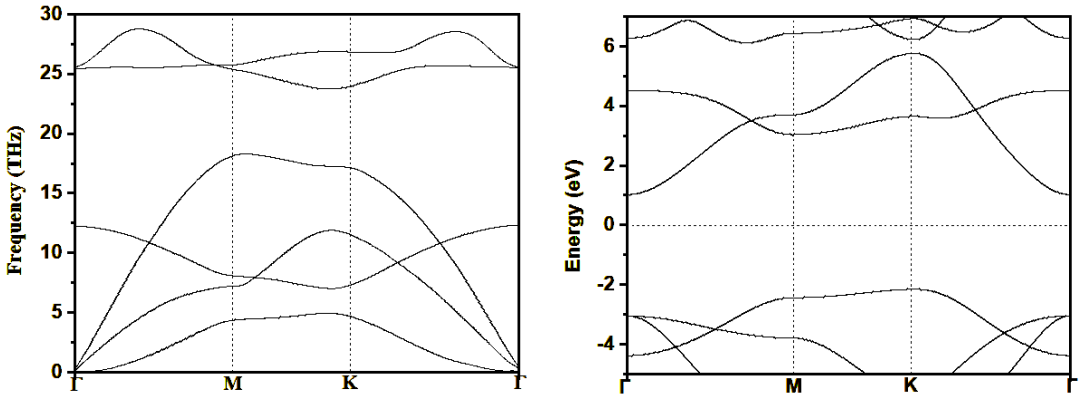

(a) (b)

FIG. 2. a) Phonon spectra and b) electronic band structure of primitive AlN nanosheet (AlNNS)

This structural reconfiguration can be attributed to electronic reorganization around the vacancy site. The three nitrogen atoms adjacent to the vacancy site, each with one unbound electron in their $2p_z$ state, undergo reorganization into $2p_x$, $2p_y$, or $2p_z$ states. This electronic rearrangement stabilizes the distorted geometry through a mechanism known

as pseudo Jahn–Teller distortion. To investigate the stability of Al/N or Al-N vacancy defects in AlNNSs, we conduct detailed calculations of the formation energy associated with these vacancy defects by the following formula:

$$E_f^i(\text{defected AlNNS}) = E_{\text{Tot}}^i(\text{defected AlNNS}) - E_{\text{Tot}}(\text{AlNNS}) + \mu(i). \tag{5}$$

In this context, $E_{\text{Tot}}^i(\text{defected AlNNS})$ represents the total energy of the supercell that contains vacancy defects in AlNNSs, while $E_{\text{Tot}}(\text{AlNNS})$ denotes the total energy of the supercell without such defects. Additionally, $\mu(i)$ signifies the chemical potential of the removed atom i(Al/N/Al–N) within the AlNNSs. The chemical potential of Al and N are calculated in the frame of fcc-Al and N_2 molecule. Calculations reveal Al-deficient and Al–N (divacant) configuration has E_f of 12.22 and 11.63 eV which is relatively larger than $E_f = 8.45$ eV of N-deficient. Suggesting creating N-vacancy is energetically relatively less favorable. The analysis of the electronic band structure (Fig. 3(a)) and density of states (PDOS) (Fig. 3(b)) in the Al-deficient configuration revealed the presence of impurity states above the valence band in the down-spin channel. These impurity states primarily arise from the non-bonding electrons of the nitrogen atoms surrounding the vacancy. In contrast, the up-spin channel maintained a wide bandgap, indicating that the aluminum-deficient AlNNS configuration behaves as a p-type semiconductor. Additionally, the structural puckering around the vacancy site led to a breaking of degeneracy in the energy levels, particularly affecting the M to K region of the lower conduction band.

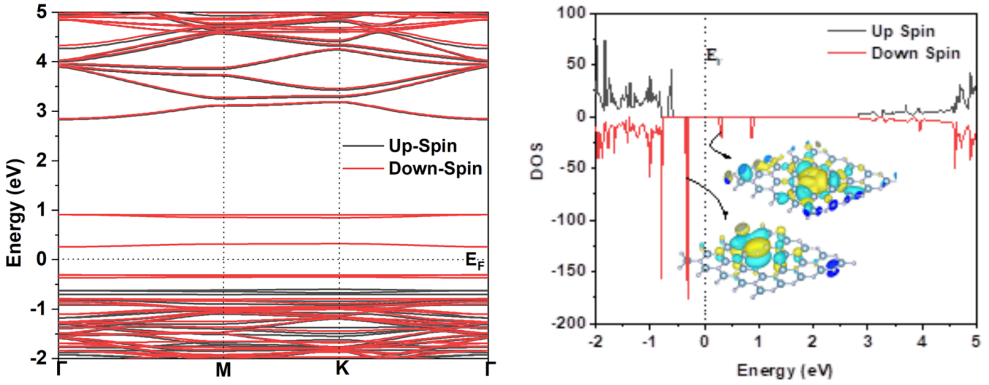

(a) (b)

FIG. 3. a) Electronic band structure and b) PDOS of Al-deficient AlNNS

In contrast to the Al-deficient configuration, the N-deficient monolayer exhibited minimal structural deformation in the vicinity of the vacancy. The primary structural change observed was a slight contraction of the nearest Al-Al distance from 3.16 to 3.15 Å at the vicinity of the defect (Fig. 1(c)). The electronic analysis indicated that the empty $2p_z$ orbitals in the under-coordinated aluminum atoms created an impurity state below the conduction band in the up-spin channel. The electronic band structure and partial density of states (PDOS) analyses (shown in Fig. 4) confirmed that the nitrogen-deficient configuration behaves as an n-type semiconductor.

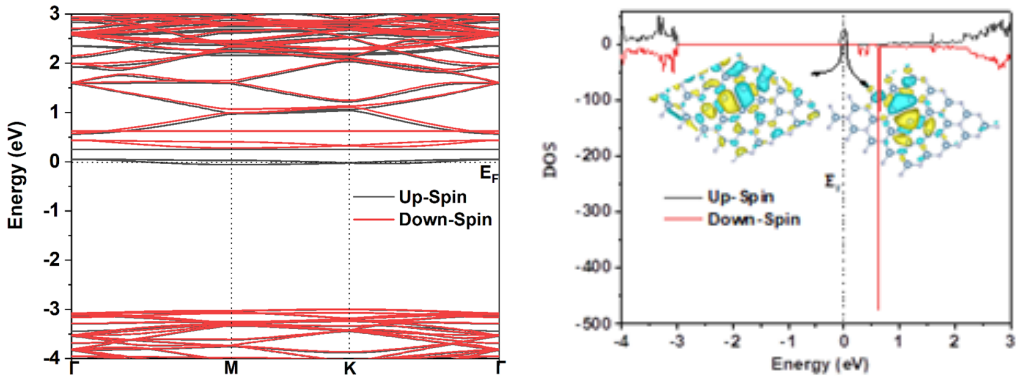

(a) (b)

FIG. 4. a) Electronic band structures and b) PDOS of N-deficient AlNNS

We further extended our investigation to include an Al–N divacancy, created by removing a nearest Al–N bond from one of the hexagonal meshes of the AlNNS. Geometrical analysis revealed significant structural modifications, particularly in the nearest N–N bond length close to the divacancy site (Fig. 1(d)), which contracted substantially from 3.16 to

2.88 Å. This configuration features six electrons from two under-coordinated N atoms and empty Al-2p_z orbitals from two under-coordinated Al atoms. These electronic characteristics generate impurity states above and below the valence band and the conduction band, respectively. The contributions from Al-2p_z orbitals appear as electronic bands above the valence state in the both up-spin and down-spin channels, while the nitrogen non-bonding electrons contribute to impurity states below the conduction band. The electronic band structure and PDOS analyses (Fig. 5) confirm that the divacant configuration maintains semiconducting behavior in the both up-spin and down-spin channels. The charge difference density plots for Al-deficient, N-deficient, and Al–N deficient AlNNS configurations are presented in Fig. S4. The charge dispersion analysis within the vicinity of the defected regions indicates that Al-deficient sites act as electrophilic centers, while N-deficient sites function as nucleophilic centers. Interestingly, the Al–N deficient sites demonstrate a competitive feature, exhibiting both electrophilic and nucleophilic characteristics. This dual functionality of the divacancy configuration suggests potential applications in biosensor development, where such sites could interact with a variety of biomolecules.

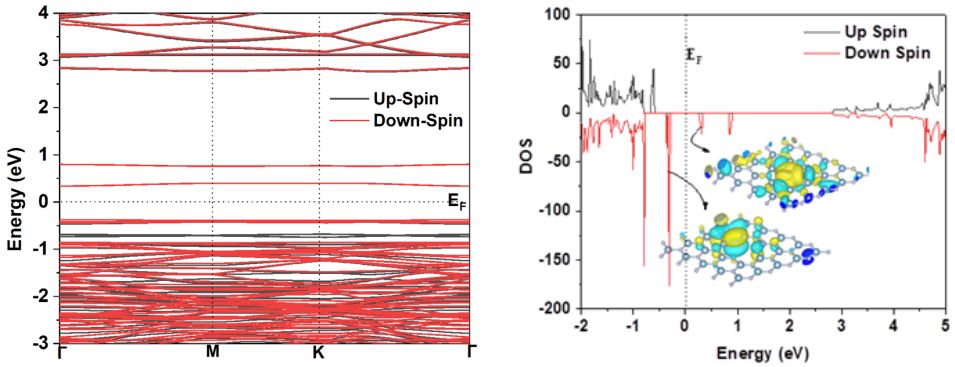

(a) (b)

FIG. 5. a) Electronic band structure and b) PDOS of Al–N-defected AlNNS

3.2. Quantum Capacitance and surface charge

Pristine aluminum nitride nanosheets (AlNNS) exhibit a wide bandgap of 2.93 eV, resulting in no available density of states near the Fermi level. According to equation (2), this characteristic prevents quantum capacitance (C_Q) from being observed within the biased window region of -1.0 to 1.0 V. However, introducing defects creates impurity states that dramatically alter the electronic structure and quantum capacitance properties of these materials. Fig. 6 demonstrates the C_Q and surface charge (Q) spectra of the studied defected AlNNS. The Al-deficient AlN monolayer demonstrates remarkable quantum capacitance properties, primarily in the positive bias region. This defect configuration shows a maximum quantum capacitance ($C_{Q\text{Max}}$) of 690 μF/cm^2 at 0.06 V (Fig. 6(a)), which is attributed to impurity states located below the Fermi level, as evidenced by the band structure and density of states (DOS) plots. Additionally, a continuous C_Q band is observed from 0.36 to 1.00 V, originating from states at the upper edge of the valence band. Surface charge analysis of the Al-deficient system reveals low charge dispersion in the negative biased region, corresponding to the observed low C_Q dispersion in this range. Following equation (4), the maximum surface charge in the positive biased region reaches 357 μC/cm^2 (Fig. 6(b)).

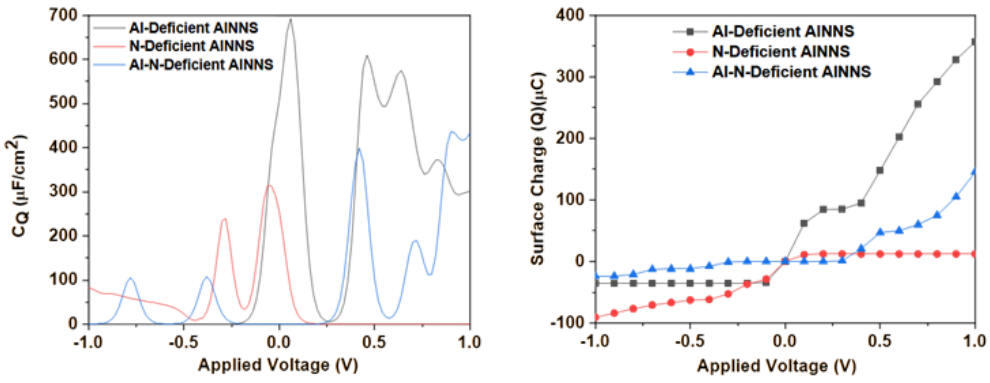

(a) (b)

FIG. 6. a) Quantum capacitance and b) surface charge of defected AlNNS at different biased voltages

These characteristics suggest that Al-deficient AlNNS could serve as an effective anode material for supercapacitor applications [27, 28]. The N-deficient AlN monolayer exhibits a quantum capacitance pattern that differs substantially from the Al-deficient variant. In this configuration, C_Q peaks are predominantly localized in the negative biased region, featuring values of 313 and 239 μF/cm^2. These peaks primarily originate from impurity states introduced by Al-2p$_z$ orbitals. The system also displays a low-valued continuous C_Q spectrum extending from -0.5 to -1.00 V, which can be attributed to the conduction band minima (CBM). This defected nanosheet has a $C_{Q\text{Max}}$ of -93 μC/cm^2, which is reasonable for it to be a cathodic candidate for supercapacitor applications. The Al–N deficient AlNNS exhibits a more complex quantum capacitance spectrum with peaks distributed across both negative and positive biased regions, though the dominant C_Q peaks appear in the positive biased region. The peaks in the positive region primarily originate from non-bonding electrons associated with nitrogen atoms, while peaks in the negative biased region stem from Al-2p$_z$ states situated below the Fermi level. The most prominent C_Q peaks for this divacant configuration reach 39 and 438 μF/cm^2 at 0.4 and 0.9 V, respectively, with a maximum surface charge ($C_{Q\text{Max}}$) of 146 μC/cm^2 in the positive biased region. This intermediate behavior between the Al-deficient and N-deficient systems offers additional flexibility for potential applications. These calculated C_Q peaks are larger than many earlier reports conducted on functionalized 2D surfaces, specifically in the positively biased region [29, 30]. In Table 1, important descriptors associated with Al, N or Al–N deficient AlNNT are shown.

TABLE 1. Different calculated characteristics of mono-vacant and di-vacant AlNNS

Atomic Configuration	Formation energy	Energy Bandgap (eV)	Maximum Quantum Capacitance ($C_{Q\text{Max}}$)	Maximum Surface Charge (Q_{Max})
Al-deficient AlNNS	11.81	0.57 eV	690 μF/cm^2	357 μC/cm^2
N-deficient AlNNS	11.16	Half-metallic	313 μF/cm^2	-93 μC/cm^2
Al–N-deficient AlNNS	8.02	0.68	438 μF/cm^2	146 μC/cm^2

4. Conclusions

This study explores the structural and electronic properties of monovacant and divacant AlNNS (Aluminum Nitride Nanostructures). Formation energy calculations indicate that these structures are feasible. The band structure and density of states (DOS) analyses show that impurity states play a significant role in describing the electronic characteristics of these monolayers. In this context, N-deficient AlNNS demonstrate a robust n-type semiconducting behavior, while Al-deficient AlNNS exhibit strong p-type characteristics. Furthermore, Al–N-deficient AlNNS stand out as wide bandgap semiconductors, showcasing the presence of both acceptor and donor energy levels. Among the different defects Al-deficient AlNNSs exhibits $C_{Q\text{Max}}$ of 690 μF/cm^2 and Q_{Max} of 357 μC/cm^2. The nitrogen-defected AlNNS demonstrates excellent performance as a cathode material with a maximum quantum capacitance of 313 μF/cm^2 and a maximum charge capacity of 91 μC/cm^2. In contrast, the aluminum-defected NS shows properties suitable for anode applications, with a maximum quantum capacitance of 32 μF/cm^2 and a maximum charge capacity of 23 μC/cm^2. The Al–N divacancy configuration exhibits an intermediate behavior with prominent quantum capacitance peaks in both biased regions, offering additional flexibility for potential applications. These findings establish defected AlN monolayers as promising electrode materials for next-generation supercapacitors, with their performance characteristics being highly tunable through defect engineering.

References

[1] Hughes Z.E., Walsh T.R. Computational chemistry for graphene-based energy applications: progress and challenges. *Nanoscale*, 2015, **7** (13), P. 6883–6908.

[2] Ponnamma D., Vijayan P., Al Ali Al-Maadeed M. 3D architectures of titania nanotubes and graphene with efficient nanosynergy for supercapacitors. *Mater. Des.*, 2017, **117**, P. 203–212.

[3] Wang G., Zhang L., Zhang J. A review of electrode materials for electrochemical supercapacitors. *Chem. Soc. Rev.*, 2012, **41** (2), P. 797–828.

[4] Pak A.J., Paek E., Hwang G.S. Relative contributions of quantum and double layer capacitance to the supercapacitor performance of carbon nanotubes in an ionic liquid. *Phys. Chem. Chem. Phys.*, 2013, **15** (44), P. 19741–19747.

[5] Stoller M.D., Magnuson C.W., Zhu Y., Murali S., Suk J.W., Piner R., Ruoff R.S. Interfacial capacitance of single layer graphene. *Energy Environ. Sci.*, 2011, **4** (11), P. 4685–4689.

[6] Xia J., Chen F., Li J., Tao N. Measurement of the quantum capacitance of graphene. *Nat. Nanotechnol.*, 2009, **4** (8), P. 505–509.

[7] Vurgaftman I., Meyer J.N. Band parameters for nitrogen-containing semiconductors. *J. Appl. Phys.*, 2003, **94** (6), P. 3675–3696.

[8] Wu J. When group-III nitrides go infrared: New properties and perspectives. *J. Appl. Phys.*, 2009, **106** (1), 011101.

[9] Zhang Y., Liu J., He R., Zhang Q., Zhang X., Zhu J. Synthesis of aluminum nitride nanowires from carbon nanotubes. *Chem. Mater.*, 2001, **13** (11), P. 3899–3905.

[10] Wu Q., Hu Z., Wang X., Lu Y., Chen X., Xu H., Chen Y. Synthesis and characterization of faceted hexagonal aluminum nitride nanotubes. *J. Am. Chem. Soc.*, 2003, **125** (34), P. 10176–10177.

[11] Stan G., Ciobanu C.V., Thayer T.P., Wang G.T., Creighton J.R., Purushotham K.P., Cook R.F. Elastic moduli of faceted aluminum nitride nanotubes measured by contact resonance atomic force microscopy. *Nanotechnology*, 2008, **20** (3), 035706.
[12] Zhang X., Liu Z., Hark S. Synthesis and optical characterization of single-crystalline AlN nanosheets. *Solid State Commun.*, 2007, **143** (6-7), P. 317–320.
[13] Lei M., Song B., Guo X., Guo Y.F., Li P.G., Tang W.H. Large-scale AlN nanowires synthesized by direct sublimation method. *J. Eur. Ceram. Soc.*, 2009, **29** (1), P. 195–200.
[14] Wang P., Wang T., Wang H., Sun X., Huang P., Sheng B., Wang X. Experimental evidence of large bandgap energy in atomically thin AlN. *Adv. Funct. Mater.*, 2019, **29** (36), 1902608.
[15] Han L., Li Y., Zhao Y., Meng X., Lei X., Yang X., Liu M. One-time mass production of AlN nanosheets: Synergistic effect of high-energy shear and effective collision in a sanding mill. *Ceram. Int.*, 2024, **50** (11), P. 19642–19649.
[16] Javaheri S., Babaeipour M., Boochani A., Naderi S. Electronic and optical properties of V doped AlN nanosheet: DFT calculations. *Chin. J. Phys.*, 2018, **56** (6), P. 2698–2709.
[17] Peng Y., Xia C., Zhang H., Wang T., Wei S., Jia Y. Tunable electronic structures of p-type Mg doping in AlN nanosheet. *J. Appl. Phys.*, 2014, **116** (4), 044306.
[18] Liu P., De Sarkar A., Ahuja R. Shear strain induced indirect to direct transition in band gap in AlN monolayer nanosheet. *Comput. Mater. Sci.*, 2014, **86**, P. 206–210.
[19] Tsipas P., Kassavetis S., Tsoutsou D., Xenogiannopoulou E., Golias E., Giamini S.A., Grazianetti C. et al. Evidence for graphite-like hexagonal AlN nanosheets epitaxially grown on single crystal Ag(111). *Appl. Phys. Lett.*, 2013, **103** (25), 251605.
[20] Perdew J.P., Burke K., Ernzerhof M. Generalized gradient approximation made simple. *Phys. Rev. Lett.*, 1996, **77** (18), P. 3865–3868.
[21] Monkhorst H.J., Pack J.D. Special points for Brillouin-zone integrations. *Phys. Rev. B*, 1976, **13** (12), P. 5188–5192.
[22] Troullier N., Martins J.L. Efficient pseudopotentials for plane-wave calculations. *Phys. Rev. B*, 1991, **43** (3), P. 1993–2006.
[23] Ordej'on P., Artacho E., Soler J.M. Self-Consistent Order-N Density-Functional Calculations for Very Large Systems. *Phys. Rev. B*, 1996, **53** (16), R10441–R10444.
[24] Soler J.M., Artacho E., Gale J.D., Garc'ia A., Junquera J., Ordej'on P., S'anchez-Portal D. The Siesta method for ab initio order-N materials simulation. *J. Phys.: Condens. Matter*, 2002, **14** (11), P. 2745–2779.
[25] The MathWorks Inc. Statistics and Machine Learning Toolbox Documentation, Natick, Massachusetts: The MathWorks Inc., 2022, URL: https://www.mathworks.com/help/stats/index.html.
[26] Nguyen D.K., Vu T.V., Hoat D.M. Antiferromagnetic ordering in the TM-adsorbed AlN monolayer (TM = V and Cr). *RSC Adv.*, 2022, **12** (26), P. 16677–16683.
[27] SanthiBhushan B., Khan M.S., Bohat V.K., Srivastava A. Quantum capacitance estimations of pyrrolic-rich graphene for supercapacitor electrodes. *IEEE Trans. Nanotechnol.*, 2018, **17** (2), P. 205–211.
[28] Hu R., Shang J. Quantum capacitance of transition metal and nitrogen co-doped graphenes as supercapacitors electrodes: A DFT study. *Appl. Surf. Sci.*, 2019, **496**, 143659.
[29] Mousavi-Khoshdel M., Targholi E., Momeni M.J. First-principles calculation of quantum capacitance of codoped graphenes as supercapacitor electrodes. *J. Phys. Chem. C*, 2015, **119** (47), P. 26290–26295.
[30] Khan Z.R., Abbas Z., Akhter N., Khan M.S., Khan M.S. Enhanced quantum capacitance in Ti, V, Cr, Fe, Ga, Ge, Se, and Br doped arsenene: a first principles investigation. *Chem. Phys. Lett.*, 2023, **823**, 140500.

Submitted 1 August 2025; revised 4 November 2025; accepted 5 November 2025

Information about the authors:

Shamsuddin Ahmad – Department of Physics, Z. A. Islamia P. G. College Siwan, Bihar-841226, India; sahmadzaic@gmail.com

Md. Mahfoozul Haque – Department of Physics, Marwari College, T. M. Bhagalpur University, Bihar-812007, India; mahfooz.haque@gmail.com

Zaheer Abbas – Department of Science and Humanities, Government Engineering College, Jehanabad, Bihar-804407, India; zaheerid@gmail.com

Md. Shahzad Khan – Department of Physics, Z. A. Islamia P. G. College Siwan, Bihar-841226, India; ORCID 0000-0001-9769-582X; kshahzad001@gmail.com

Conflict of interest: the authors declare no conflict of interest.

Data availability statement: The data is available upon request.

Author contribution: The authors confirm contribution to the paper as follows: Dr. Shamsuddin Ahmad has conceptualized, collected data and analyzed the work. Dr. Md. Mahfoozul Haque has reviewed and analyzed, Dr. Zaheer Abbas helped in interpretation of results. Dr. Md. Shahzad Khan has written, reviewed and supervised the work.